Supplementary Information for:

Protons crossing triple phase boundaries based on a metal catalyst, Pd or Ni, and barium zirconate

Massimo Malagoli[1], M.L. Liu[2], Hyeon Cheol Park[3], and Angelo Bongiorno[1]

June 5, 2013

[1]*School of Chemistry & Biochemistry, Georgia Institute of Technology,*
Atlanta, Georgia 30332-0400
[2] *School of Material Science & Engineering, Georgia Institute of Technology,*
Atlanta, Georgia 30332-0245
[3] *Advanced Materials Research Center Samsung Advanced Institute of Technology (SAIT),*
San 14-1, Nongseo-dong, Yongin-si 446-712, Republic of Korea

1. Computational approach

1.1 Method

In this study, we performed density functional theory (DFT) calculations by using the Vienna Ab-initio Simulation Package (VASP) [1, 2]. This DFT scheme relies on plane-wave basis sets to represent wave-functions and the electronic charge density. To describe the interaction of valence electrons and ionic cores, we used the projector augmented wave method (PAW) [3, 4]. Further, we used the revised form [5] of the Perdew-Burke-Ernzerhof functional [6] to account for the exchange and correlation energy.

Convergence tests showed that the oxide and metallic materials considered in this study are described well by using a plane-wave energy cutoff of 400 eV (Table S1). In this work, perfect bulk materials were modeled by using small supercells and dense k-point meshes in the Brillouin zone. DFT calculations of defected bulk systems, and surface and interface models were based on large supercells and the Brillouin zone was thus sampled only at the Γ-point.

Table **S1**: Total energy in eV (top) and volume in Å^3 (bottom) of a primitive unit cell of $BaZrO_3$ vs. plane-wave energy cutoff and density of the Monkhorst-Pack *k*-point mesh in the Brillouin zone.

k-point mesh	Energy cutoff (eV)					
	300	400	500	600	700	800
3×3×3	-42.370	-41.348	-41.304	-41.312	-41.324	-41.329
4×4×4	-42.470	-41.408	-41.363	-41.371	-41.382	-41.388
5×5×5	-42.493	-41.419	-41.372	-41.380	-41.391	-41.396
6×6×6	-42.496	-41.421	-41.373	-41.381	-41.393	-41.398
3×3×3	69.99	76.73	78.56	78.53	78.50	78.58
4×4×4	69.96	76.61	78.50	78.43	78.40	78.48
5×5×5	69.99	76.61	78.49	78.45	78.42	78.50
6×5×5	70.02	76.75	78.48	78.45	78.42	78.50

$BaZrO_3$ (BZ) has the ideal cubic perovskite structure with space group $Pm\overline{3}m$. At low temperature, the measured lattice constant, bulk modulus, and static dielectric constant are 4.191 Å, 152 GPa, and 45-47, respectively [7, 8]. Our DFT calculations give values for the same quantities of 4.25 Å, 144 GPa, and 51 (ε_∞=4.9), respectively. The Kohn-Sham band gap of BZ is 3.1 eV, as expected ∼40% smaller than the experimental value of 5.3 eV [9]. Lattice constants and bulk moduli of Pd and Ni obtained from DFT are 3.99 Å and 150 GPa, and 3.53 Åand 179 GPa, respectively. These latter values compare well with experimental data. Overall, these results show that our DFT scheme describes well $BaZrO_3$, Pd, and Ni materials.

1.2 Modeling approach

Materials in fuel cells and electrochemical processes occurring near "triple phase boundaries" (TPBs) involve multiple scales. Capturing the full complexity of a TPB via DFT is unrealistic. However, DFT calculations have the ability to provide atomistic insight on well-selected aspects of these highly inhomogeneous and articulated systems. In our work, DFT was used to address the energetics of hydrogen species crossing TPBs based on yttrium-doped barium zirconate (BZY). In particular, we focused on TPBs based on either Pd or Ni and BZY, and we investigated the energetics of the following key elementary process:

$$\mathrm{H}^*[metal] \rightarrow \mathrm{H}^+[BYZ] + e^-, \tag{1}$$

leading to the transfer of a hydrogen species (H^*) from the metallic to the electrolyte component of TPBs based on barium zirconate (BZ). The reaction above occurs near the TPB, at the interface between the metal catalyst and electrolyte, and its final state consists of a a proton (H^+) incorporated into the ceramic and an electron (e^-) transferred to an acceptor state near the TPB. Reaction 1 may follow different pathways. In this work, we investigated reaction 1 under the assumption that the proton incorporation step is accompanied by an electron transfer step to the metallic component of the TPB. We disregarded the effect of voltage bias and we addressed the energetics of reaction 1 by assuming an equilibrium situation for materials and TPBs at open circuit voltage. Validity and significance of our results are further defined by the following aspects.

- Our DFT scheme is based on a generalized gradient approximation of the exchange and correlation energy [5]. This standard DFT approach reproduces – with errors of a few percent with respect to experimental data – structural, dynamical, dielectric, and chemical bonding characteristics of the materials and molecules investigated in this study. Band structure and energy gap of barium zirconate are subjected to larger errors. To some extent, this inaccuracy reflects on the quantities calculated in our work, i.e. proton formation energies and Schottky barriers. Consequently, the results of this computational study are expected to have qualitative value and to be quantitatively approximated.

- The equilibrium energy of a protonic defect in BZY depends on the value of the Fermi level in the band gap (see below). In this study, we assumed BZY materials with a very low concentration of acceptor states, and thus a Fermi level positioned at mid-gap. The computed Kohn-Sham band gap of $\mathrm{BaZrO_3}$ is 3.1 eV (∼40% smaller than the experimental value of 5.3 eV [9]). Thus, we positioned the Fermi level in BZY 1.55 eV above the valence-band maximum. We remark that, regardless the value of the Fermi level in the gap of BZY, protons are – in agreement with the experiment – always more stable than neutral hydrogen species in this material.

- We computed zero-temperature energies of hydrogen species far from a TPB, on the surface and in the bulk of both metal catalysts and BZY, and in the near-surface region of the electrolyte in direct contact with the metal and gas phase. We did not account for the vibrational entropy of hydrogen defects at surface, interface, or bulk sites, and we derived our conclusions by comparing relative enthalpy values. We remark that free energy terms accounting for the vibrational entropy of hydrogen defects at confined sites in materials are expected to be small and, most importantly, comparable.

- To reduce both computational cost and scope of our study, we did not investigate the effect of Y dopants on both the nature of the metal-electrolyte interface and the energy of protons in the near-interface layers of the oxide. We therefore assumed and modeled that the transfer of a proton from the metal to the electrolyte was accompanied by an electron transfer process to the metal component of the TPB.

In accord with the experiment, our study showed that protonic species in BZ are more stable on the surface than in the bulk, that hydrogen species in Ni and Pd are more stable on the surface than in the bulk of these metals, and that the solubility of hydrogen in Pd is larger than in Ni. These results are consistent with qualitative expectations based on chemical intuition. We remark that a direct comparison with the experiment based on absolute values of the defect energies obtained from DFT is challenging, due to systematic errors introduced in the calculated quantities by the approximated energy scheme, which is based on pseudopotentials, a parametrized exchange-correlation functional, and a truncated basis set [10].

1.3 Defect formation energy

In this work, the energy of a hydrogen species at surface, interface, and bulk sites of our materials was calculated by using the following equation:

$$\Delta E_H^q = E_0(H,q) - E_0 - \mu_H + q\varepsilon_f, \tag{2}$$

where $E_0(H,q)$ is the total DFT energy of the defected material system including a hydrogen species in the charge state q, E_0 is the total energy of the perfect system, and μ_H and ε_f are the chemical potentials for the hydrogen atoms and electrons, respectively. In this study, we took μ_H equal to half the energy of a H_2 molecule. Further, the Fermi energy in BZY was assumed to lie at mid-gap. This value of ε_f was used to compute the energy of hydrogen species in the bulk and on the surface of BZY. On the surface and in the bulk of metals, hydrogen is present in the form of screened proton, and in this case

ΔE_H^0, ΔE_H^+, and ΔE_H^- were found to be all equal. To calculate the energy of protonic species at the interface between metals and BZY, we computed ΔE_H^0.

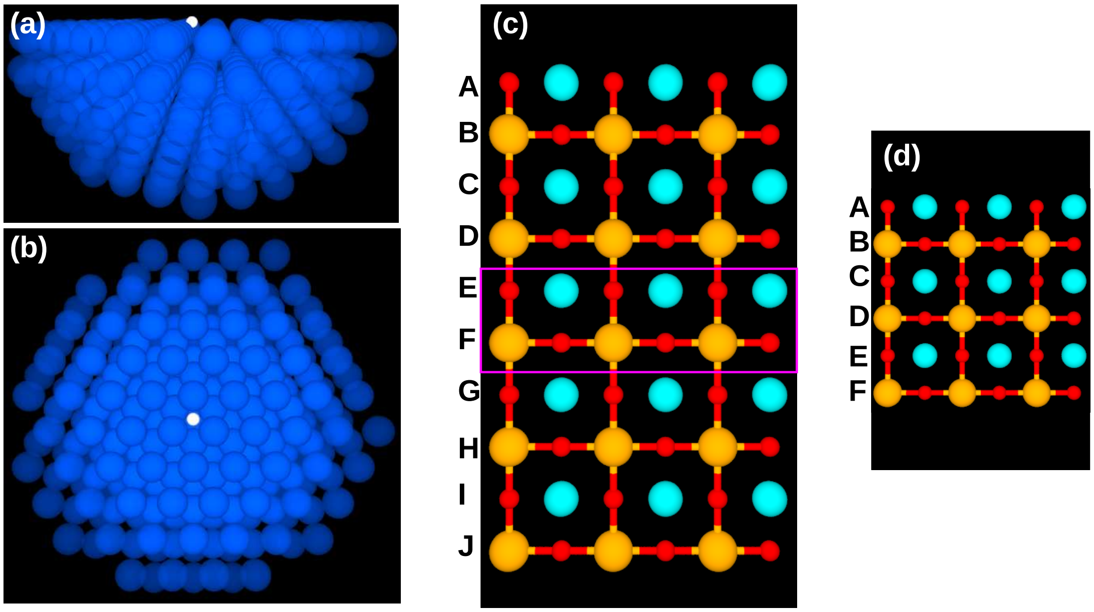

Figure **S1**: **H on Pd(111) and slab model structures of BZ. (a)** Side and **(b)** top views of a hydrogen species adsorbed on the Pd(111) surface. **(c)** Slab model used to represent the (001) surface of BZ. Capital letters A through J are used to label the layers of the slab; A and J correspond to the BaO and ZrO_2 terminal layers of the slab. **(d)** Slab model of a BZ(001) surface used to represent the electrolyte component of TPBs. Layers are labeled with capital letters. A and F are the BaO and ZrO_2 terminations, respectively. Ba, Zr, O, and Pd atoms are shown in cyan, orange, red, and blue colors, respectively.

Due to the use of the supercell method, our DFT calculations of charged defects make use of a uniform charge background to neutralize the infinite and periodic material system. The electrostatic interaction of an array of point-like charged defects and the uniform charge background is – as discussed in Refs. [11, 12] – equal to:

$$E_c = -\frac{\alpha q^2}{2\varepsilon L}, \tag{3}$$

where q denotes the defect charge, α the lattice-type dependent Madelung constant, ε the macroscopic dielectric constant of the material hosting the defect, and L the supercell lattice constant. Due to the values of L and ε of the materials systems modeled in this study, the energy correction, E_c, to the Eq. 2 amounts to no more than 0.1 eV. For this reason, E_c was not accounted for in this study.

2. Hydrogen in the bulk of BZY

We calculated the energy of both a neutral hydrogen species and a proton in BZY. Perfect BZ and Y-doped BZ were modeled by using supercells consisting of either 3×3×3 or 4×4×4 primitive unit cells of BZ including 0 and up to 2 substitutional Y dopants, respectively. These model structures of BZY represent $BaZr_{1-x}Y_xO_3$ materials with x between 0 and 0.074. Typical experimental values of x range between 0.05 and 0.2 [13]. Our models and results therefore account for the effect of Y-dopants on the energetics of protons in mildly doped BZY materials.

We found that H^+ is the most stable species in BZY, regardless both the doping levels considered in this study and the value of ε_f in the band gap. In perfect BZ, we obtained energies for H^+ of 0.59 eV and 0.54 eV by using supercells of 3×3×3 and 4×4×4 unit cells, respectively. The complete list of energy values obtained for both a neutral and positively charged hydrogen species in our BZY models is reported in Table S2.

3. Hydrogen in the bulk and on the surface of Pd and Ni

To model the bulk phases of Pd and Ni, we used cubic supercells consisting of 108 metal atoms on a fcc lattice, and a 2×2×2 Monkhorst-Pack grid of k-points in the Brillouin zone. Surface calculations were performed by using slab models consisting of a stack of 6 (111) layers, each one with a periodic area of (4×4) surface unit cells. The two symmetric faces of the slabs were separated by a vacuum region of about 10 Å. To model the occurrence of a bulk region, the atoms of the two central layers of the slab were held fixed at their ideal bulk lattice positions. Hydrogen is these metals is present in the form of screened proton. The calculation of ΔE_H^0 and ΔE_H^+ gives indeed the same result. Fig. S1 shows a hydrogen atom adsorbed on the Ni(111) surface.

4. Hydrogen on (001) surfaces of BZY

Surface calculations were performed by using slab models within our supercell method (Fig. S1). We considered the (001) surface of $BaZrO_3$ and we used slabs consisting of 3×3×5 unit cells of BZ (Fig. S1(c)). The slab model is periodic in the xy-plane, and in the z-direction, the opposite BaO and ZrO_2 terminations of the slab are separated by a vacuum region of 10 Å(Fig. S1). The two terminations of the BZ(001) surface are apolar [14] and thermodynamically stable [15]. The energies of H^+ obtained by using the slab

Table **S2**: Energy (in eV) of H^0 (ΔE_H^0) and H^+ (ΔE_H^+) in BZY. The results are obtained by using Eq. 2 and DFT calculations based on supercells including 3×3×3 and 4×4×4 primitive unit cells of BZ and up to 2 substitutional Y defects. The distances (d) between the two Y dopants, and between the protonic defect (OH) and the two Y ions are in Å and have been extracted from the fully optimized model structures of BZY. In the neutral state, H^0 yields the electron to BZY, filling an acceptor level in the valence band and therefore becoming a protonic defect. The small energy differences obtained for a neutral and positively charged hydrogen in BZY giving rise to the same configuration for a protonic species stem from the occurrence of the filled acceptor-state in the case of the neutral system.

x	d(Y$_1$-Y$_2$)	d(HO-Y$_2$)	d(HO-Y$_1$)	ΔE_H^0	ΔE_H^+
0.016	-	-	2.30	0.40	0.38
0.016	-	-	13.59	0.66	0.55
0.037	-	-	2.29	0.38	0.34
0.037	-	-	4.78	0.49	0.44
0.037	-	-	6.39	0.53	0.46
0.037	-	-	6.44	0.51	0.44
0.037	-	-	7.68	0.51	0.46
0.037	-	-	8.79	0.52	0.45
0.074	4.30	2.24	2.25	0.14	0.15
0.074	4.30	8.78	8.79	0.49	0.48
0.074	6.03	2.32	4.77	0.44	0.38
0.074	6.03	8.82	8.81	0.66	0.55
0.074	7.39	2.31	6.35	0.36	0.37
0.074	7.39	6.42	8.50	0.49	0.49

model shown in Fig. S1(c) are reported in Table S3. In these DFT calculations, structural optimizations were carried out by fixing the geometry of the two central layers of the slab as in bulk BZ. Structural optimization of the undefected slab led to relaxations of the surface layers in excellent agreement with those reported in Ref. [15]. In a few well-selected cases, we repeated the calculation of ΔE_H^+ by using symmetric BZ(001) slabs terminated by a BaO or ZrO_2 layer. These two slab models were obtained from those shown in Fig. S1(c) by removing the layer labeled J and A, respectively. In these calculations, structural optimizations were carried out by fixing the positions of the atoms belonging to the central layer of the slab. These calculations led to defect energies differing by less than 0.1 eV from those reported in Table S3, confirming that the defect energies reported in Table S3 are influenced very little by the geometry of our slab model.

To allow the comparison of bulk and surface defect energies, the Fermi levels resulting from the two types of supercell calculations needed to be aligned [16]. In detail, the Fermi energy, ε_f^s, used in Eq. 2 to calculate surface defect energies was obtained from:

$$\varepsilon_f^s = \langle V \rangle_s + \varepsilon_f - \langle V \rangle, \tag{4}$$

where $\langle V \rangle$ and ε_f are the energy values of the average electrostatic potential and Fermi level in the bulk of BZ, while $\langle V \rangle_s$ is the macroscopic average of the electrostatic potential obtained by averaging over the central region of the slab model shown in Fig. S1(c).

Table **S3**: Energy of H^+ (in eV) obtained by modeling the BZ(001) surface through the use of the slab model shown in Fig. S1(c). Surface layers are labeled as in Fig. S1(c). Labels A and J refers to protonic species at the BaO and ZrO_2 terminal layers of the slab, respectively.

Layer	A	B	C	D	E	F	G	H	I	J
ΔE_H^+	-2.14	-0.97	-1.40	-1.07	-0.97	-0.96	-0.97	-1.38	-0.96	-2.60

5. Hydrogen at TPBs based on Pd, Ni, and BZY

The TPB region of anodes based on Pd-BZY and Ni-BZY were modeled as shown in Fig. S2. In all the cases, we used the BZ(001) slab shown in Fig. S1(d) to model the electrolyte. This slab is composed by 3×3×3 primitive unit cells, it is periodic in the xy plane, and it forms a contact with the metallic component on the (001) terminations (Fig. S2). This slab is devoid of both Y dopants and oxygen vacancies. The metallic component of the TPB was modeled by considering a single atom in contact with the surface, a 48-atom cluster sandwiched between the opposite BaO and ZrO_2 terminations of the slab, and a 24-atom cluster in contact with only the ZrO_2-terminated (001) surface of the slab (Fig. S2).

The TPB models shown in Figs. S2(b), (c), and (d) were used to calculate the energy of a protonic species in the near-surface region of the electrolyte in contact with either a Pd or Ni catalyst. These calculations were carried out by adding a neutral hydrogen species to the TPB models in Figs. S2(b), (c), and (d). Defect energies were thus obtained by using Eq. 2 to calculate ΔE_H^0. A Bader analysis of atomic charges [17] showed in all cases

Table **S4**: Energy of a protonic species in a BZY electrolyte near the interface with a metallic cluster. Energy values have been obtained by using the TPB models shown in Fig. S2(b), S2(c), and S2(d). For each layer of the BZ(001) slab (see Fig. S1(c)), we considered a protonic species in three different positions, near the center (Metal), periphery (Metal/vacuum), and outside (Vacuum) the projection perpendicular to the BZ surface of the metal/oxide interfacial area.

Pd-BZ: model in Fig. S2(b)				
	Metal	Metal/vacuum	Vacuum	Mean value
A	-0.01	-0.89	-0.62	-0.51
B	0.28	0.24	0.27	0.26
C	0.39	0.07	0.30	0.25
D	0.23	0.21	0.25	0.23
E	0.26	0.25	0.60	0.37
F	-0.20	-0.76	-0.57	-0.51
Pd-BZ: model in Fig. S2(c)				
Layer	Metal	Metal/vacuum	Vacuum	Mean value
C	0.83	0.84	0.86	0.84
D	0.72	0.74	0.73	0.73
E	0.79	0.58	0.66	0.67
F	0.42	0.17	-0.25	0.11
Ni-BZ: model in Fig. S2(d)				
Layer	Metal	Metal/vacuum	Vacuum	Mean value
A	0.81	-0.37	0.01	0.15
B	-0.49	0.91	0.85	0.42
C	0.98	0.82	0.83	0.87
D	0.82	0.83	0.82	0.82
E	1.03	0.75	0.82	0.87
F	0.69	-0.64	0.07	0.04

that hydrogen occurs as proton in the electrolyte component of the model TPBs, and that an electron is transferred to the metallic cluster. The complete list of defect energies is reported in Table S4. For each TPB model, the defect energies follow well-defined trends: high variability for protonic species bonded to superficial O ions in direct contact with the metal, and an almost constant energy value in the case of protonic species belonging

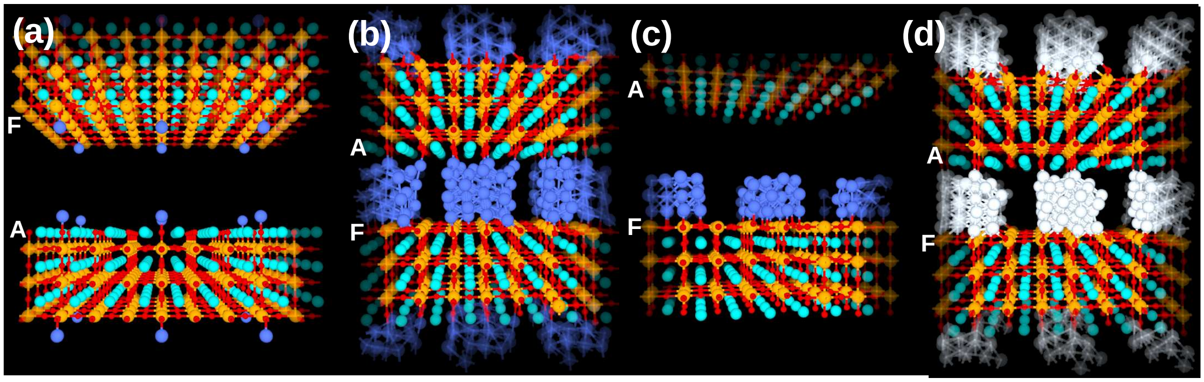

Figure **S2**: **Model structures of TPBs.** **(a)** Illustration of the simplest model structure used to study TPBs based on BZY: a 3×3×3 slab modeling the BZ(001) surface with one metal atom adsorbed on both the opposite terminations of the slab. We considered both Pd and Ni atoms in contact with the slab model. **(b)** Illustration of a realistic TPB based on BZY and Pd. In this case, the metal component consists of a 48-Pd metal cluster sandwiched between the two terminations of the slab. **(c)** The BZ(001) slab in contact with a 24-Pd cluster supported by the ZrO_2 surface termination. **(d)** The same model structure of a TPB as in (b) with a 48-Ni cluster replacing the 48-Pd cluster. Ba, Zr, O, Pd, and Ni atoms are shown in cyan, orange, red, blue, and white colors, respectively. The illustrations highlight the periodic nature of our TPB models and calculations. These model TPBs are based on the slab model for BZ(001) shown in Fig. 1(c). The layers of this slab are indicated in Figures and Tables as shown in Fig. 1(c). For clarity, the terminal layers of the slab are also indicated in this figure.

to the BZ layers beneath. This latter energy value is controlled by the Schottky energy barrier formed by metal-electrolyte junction.

Schottky barrier heights were calculated by referring the Fermi level of the metallic cluster to the value of valence-band edge in the central region of the slab model of the electrolyte [16]. This latter value was calculated – as in the case of the surface calculations – by aligning the macroscopic electrostatic potentials obtained from the bulk calculation of perfect BZ and that one obtained by averaging over the central region of the BZ slab [16].

References

[1] G. Kresse and J. Furthmüller, Comput. Mater. Sci. **6**, 15 (1996)

[2] G. Kresse and J. Furthmüller, Phys. Rev. B **54**, 11169 (1996)

[3] P. E. Blöchl, Phys. Rev. B **50**, 17953 (1994)

[4] G. Kresse and D. Joubert, Phys. Rev. B **59**, 1758 (1999)

[5] Y. Zhang and W. Yang, Phys. Rev. Lett. **80**, 890 (1998)

[6] J. P. Perdew, K. Burke, and M. Ernzerhof, Phys. Rev. Lett. **77**, 3865 (1996)

[7] A. R. Akbarzadeh, I. Kornev, C. Malibert, L. Bellaiche, and J. M. Kiat, Phys. Rev. B **72**, 205104 (2005)

[8] K. Goretta, E. Park, R. Koritala, M. Cuber, E. Pascual, N. Chen, A. de Arellano-López, and J. Routbort, Physica C **309**, 245 (1998)

[9] J. Robertson, J. Vac. Sci. Technol. B **18**, 1785 (2000)

[10] S. Xu, P. Sood, M. Liu, and A. Bongiorno, Appl. Phys. Lett. **99**, 181901 (2011)

[11] G. Makov and M. C. Payne, Phys. Rev. B **51**, 4014 (1995)

[12] C. Freysoldt, J. Neugebauer, and C. G. V. de Walle, Phys. Rev. Lett. **102**, 106402 (2009)

[13] K. D. Kreuer, Annu. Rev. Mater. **33**, 333 (2003)

[14] M. Stengel, Phys. Rev. B **84**, 205432 (2011)

[15] N. Iles, F. Finocchi, and K. D. Khodja, J. Phys.: Condens. Matter **22**, 305001 (2010)

[16] M. Peressi, N. Binggeli, and A. Baldereschi, J. Phys. D: Appl. Phys. **31**, 1273 (1998)

[17] W. Tang, E. Sanville, and G. Henkelman, J. Phys.: Compute Mater. **21**, 084204 (2009)